Fizika Nizkikh Temperatur, 2010, v. 36, Nos. 10/11, p. 1098–1106

Macroscopic quantum phenomena in Josephson structures

A. Barone

Dip. Scienze Fisiche, Facoltá di Ingegneria, Universitá di Napoli Federico II
Piazzale Tecchio 80, Napoli 80125 and CNR-SPIN Napoli, Italy
E-mail: barone@na.infn.it

F. Lombardi

Quantum Device Physics Laboratory, Dept. of Microtechnology and Nanoscience
Chalmers University of Technology, SE-412 96, Goteborg, Sweden

G. Rotoli and F. Tafuri

Dip. Ingegneria dell'Informazione, Facoltá di Ingegneria, Seconda Universitá di Napoli
via Roma 29, Aversa (CE) 81031 and CNR-SPIN Napoli, Italy

Received April 13, 2010

The Josephson effect is a probe of unparalleled performances in the study of a variety of macroscopic quantum phenomena. In the present article an overview of important achievements and challenging trends is given referring, in particular, to macroscopic quantum tunneling and energy level quantization. The attention is mainly addressed to high-T_C superconducting structures and recent investigations concerning nanostructures.

PACS: **74.72.–h** Cuprate superconductors;
74.81.Fa Josephson junction arrays and wire networks;
75.20.–g Diamagnetism, paramagnetism, and superparamagnetism.

Keywords: macroscopic quantum phenomena, Josephson structures.

1. Introduction

The importance of the Josephson effect [1–5] is widely recognized for both the intrinsic relevance in the context of superconductivity and for the large variety of realized and potential applications. The Josephson effect still plays a fundamental role in various challenging topics such as that of a powerful probe of the symmetry of the order parameter characterizing different classes of superconductive materials. There are various aspects of the Josephson effect of paramount importance in the context of macroscopic quantum phenomena. Among these, the quantum decay via macroscopic quantum tunneling (MQT) deserves great attention as well as the energy level quantization (ELQ) and other phenomena proper of quantum mechanics at a macroscopic level, as the occurrence of macroscopic quantum coherence in a Superconducting Quantum Intereference Device (SQUID). Let us recall that also weakly coupled Bose-Einstein condensates (BEC) systems are subject of deep theoretical and experimental investigations on both interference phenomena and the occurrence of Josephson effect [6].

The nature of superconductivity in oxide compounds lies in the background with its still mysterious origin. The phenomenology of HTS encompasses a wide range of interesting issues at the border of our understanding of solid-state systems and at the limit of current capabilities of material science and nano-technology. The Josephson junctions have been playing an irreplaceable role in defining crucial properties of HTS. The *d*-wave order parameter symmetry (OPS) is probably the most remarkable example [7,8]. If we imagine to be a few months before the discovery of HTS, who would have imagined that in a few months a supercurrent would have flown up to about 100 K? Who would have imagined a supercurrent between two phase coherent electrodes up to about 100 K? What about the thermal energy, the gap value, the Josephson coupling energy, the charging energy, the coherence length, the critical stoichiometry, and so on? These considerations lead to the first obvious feature, which is independent of the still

mysterious origin of superconductivity in HTS, of their very complicate structure, and so on: oxides enlarge the occurrence of superconductivity to unexpected energy and length scales. In this short review we try to give the feeling of novel flavors of HTS on the Josephson effect, with special attention to macroscopic quantum phenomena and to mesoscopic effects.

2. Thermal and macroscopic quantum tunneling activation

Quantum tunnelling on a macroscopic scale was considered by Sidney Coleman [9] in the context of ground state metastability in the cosmological frame. The fate of the false vacuum, was interpreted as its decay through barrier penetration, toward true vacuum, a more stable state of the Universe. In the Josephson junction cosmolab analogy, the macroscopic degree of freedom is the relative phase, ϕ, between the two weakly coupled superconductors (or the trapped magnetic flux, Φ, in a rf SQUID superconducting loop). Let us consider the potential:

$$U = -\Phi_o / (2\pi)(I_{CO}\cos(\phi) + I\phi). \qquad (1)$$

(in Fig. 1 a small section of the washboard potential is shown to focus on a single cell of the periodic structure, used later to formulate the macroscopic quantum tunneling problem) given by the sum of the free energy associated to the Josephson junction barrier and a linear term in ϕ due to the bias current I. I_{CO} represents the maximum Josephson current. This potential can be also easily derived from the the resistively and capacitively shunted junction (RCSJ) model applied to a Josephson junction. The Josephson inductance L_J and capacitance C act as an anharmonic LC resonator (at zero voltage) with resonance frequency $\omega_P = (L_J C)^{-1/2}$ (plasma frequency), where $L_J = \Phi_O / (2\pi I_{CO}\cos(\phi)) = \Phi_O / (2\pi[I_{CO}^2 - I^2])^{1/2}$, $\omega_P = (2\pi I_{CO} / (\Phi_O C)) / (1-(I/I_{CO})^2))^{1/4}$. Representing the displacement current by a C capacitor and the sum of the quasi-particle and insulator leakage current by a resistance (R), we can devise an equivalent circuit for the junction:

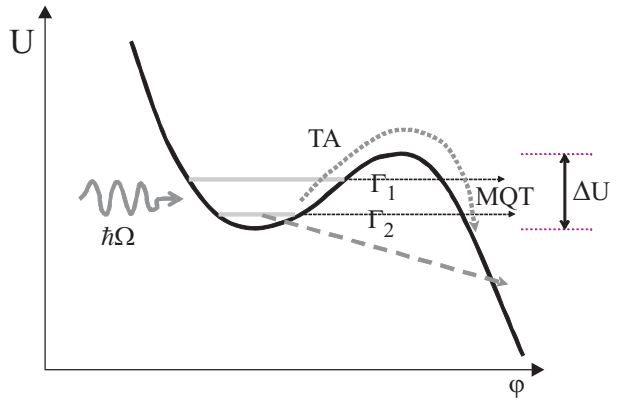

Fig. 1. Detail of the washboard potential in the RCSJ model for a finite value of the bias. ΔU represents the energy barrier. TA stands for thermal activation (dotted line), MQT processes are indicated for small (solid line) and large (dashed line) dissipation [15] both from the ground state and the first excited state, respectively. Microwaves can induce a transition from the ground to the first exited state.

$$I + I_N = I_{CO}\sin(\phi) + V/R + CdV/dt. \qquad (2)$$

The second term contains the well-known dc Josephson equation $I_C = I_{CO}\sin(\phi)$. The noise source I_N is associated with its shunt resistance.

In the mechanical analogy of this problem we can refer to a particle of mass $m = (\Phi_O / 2\pi)^2 C$ in such a washboard potential (see Eq. (1)) and identify the two states corresponding to the particle at rest (ϕ constant) or running down the slope (ϕ time-dependent). The motion of the particle is subject to damping given by $1/Q$, where $Q = \omega_P RC$ is the quality factor. Accordingly, from the constitutive Josephson effect relations, these states will correspond in the current-voltage (I–V) characteristics to the zero voltage and the finite voltage state respectively. At zero temperature such a transition will occur as soon as the average slope of $U(\phi)$ increases up to a value producing the absence of valleys (i.e. when the current bias reaches the I_C value) so that the particle can run down the slope. Namely, ϕ becomes time-dependent and the switching to the finite voltage state of the I–V curve occurs.

Depending on the entity of dissipation, conditions of overdamping with single-valued I–V curves to underdamping generating highly hysteretical I–V curves can be realized. In the former case, the large dissipation will restore the $V = 0$ state as soon as the current bias is reduced down to the critical value while, in the underdamped regime, the effect of the junction capacitance is dominant over dissipation. The mechanical analogy, is obvious referring to the interplay between the values of the friction and the inertial mass of the particle.

In the pure thermal regime, the escape rate for weak to moderate damping ($Q > 1$) is determined by the original Kramer theory as

$$\Gamma_t = A\frac{\omega_P}{2\pi}\exp\left(-\frac{\Delta U}{k_B T}\right)$$

where $\Delta U(a) = (4\sqrt{2}/3)E_J(1-\gamma)^{3/2}$ is the barrier height and is shown in Fig. 1 for $\gamma = I/I_{C0}$ close to 1, with $E_J = I_{C0}\Phi_0/2\pi$. The prefactor A can be specified accordingly to the various damping regimes. The escape rate will be dominated by MQT at low enough temperature [11,12]: for $Q > 1$ and γ close to 1 it is approximated by the expression for a cubic potential:

$$\Gamma_q = a_q\frac{\omega_P}{2\pi}\exp\left[-\frac{\Delta U}{\hbar\omega_P}\left(1+\frac{0.87}{Q}\right)\right]$$

where $a_q = [864\pi\Delta U / \hbar\omega_P]^{1/2}$. The occurrence of such a quantum activation observed in Josephson junctions shows the validity of quantum mechanics at a macroscopic level involving indeed a macroscopic variable, namely the relative phase ϕ. A complementary quantum phenomenon lies in the existence of quantized energy levels (ELQ). Evidence of such a feature is provided by the experiments based on the microwave irradiation with consequent energy level hopping.

Macroscopic quantum tunnelling in the context of the Josephson structures were proposed by Anderson [2], Ivanchenko and Zilberman [11] and by Caldeira and Leggett [12], who gave a quite complete description introducing the fundamental aspect of the effect of dissipation. The crossover temperature between the thermal and the quantum regimes is $T_{\rm cr} = (\hbar\omega_P / 2\pi k_B)[(1+1/4Q^2)^{1/2} - 1/2Q]$ [13]. Below $T_{\rm cr}$ quantum effects are dominant over thermal ones [12,14]. A variety of successful experimental investigations have been carried out to observe MQT and verify the effect of dissipation in reducing the decay rate by quantum activation [16,18]. Evidence of the transition from thermal to quantum activation was clearly shown by pioneering experiments concerning the measure of the decay rate which decreases with the temperature down to $T_{\rm cr}$ while, for $T < T_{\rm cr}$, a temperature independent activation prevails. For an excellent description of experiments in this context the reader is referred to the paper by John Clarke et al. [19]. A further issue deserving interest lies in the phenomenon of resonant macroscopic quantum tunneling (RMQT) [20] resulting in the occurrence of sharp voltage peaks due to a MQT process between levels in neighbouring wells characterized by close energy values. This effect has been experimentally confirmed by Rouse, Han and Lukens [21] in a SQUID. Concerning the Macroscopic Quantum Coherence (MQC), examples of relevant proposals and experiments can be found in [22–24].

3. Macroscopic quantum tunneling in HTS

In recent years, the interest in superconducting quantum devices has been extended to high critical temperature superconductors (HTS) also in view of the possible advantage of *d*-wave OPS [7,8] for a quiet qubit [25]. This implies the possibility of build so-called π-junction devices. The local magnetization in π-loops, i.e., loops formed with an odd number of π-junctions, could be used as the states of a qubit device. The main advantage of such an unconventional qubit device is that it works in absence of an external field bias.

Such properties of HTS devices could be also related to the search for a «protected qubit». This last can be traced to the seminal work of A.Yu. Kitaev [26] and applied to superconducting qubits by L.B. Ioffe et al. [25,27]. The basic idea is that a topological object, say a magnetic «flux» configuration over an array of Josephson junctions could have just at the classical level before the quantum effects came into play, has the property of to be insensitive to some perturbations which are topological invariant of the system.

The use of topology for making a robust qubit, i.e., insensitive to external world, can be found in the experiments by Wallraff et al. [28]. They have shown that also fluxons in annular Josephson junctions can behave as quantum objects at low temperature and could be used in principle as qubits when subject to a magnetic field induced potential [29].

HTS may be an interesting reference system for novel ideas on key issues on coherence and dissipation in solid state systems because of their unusual properties, in particular the presence of low energy quasi-particles due to nodes in the *d*-wave OPS [30,31]. This has represented since the very beginning a strong argument against the occurrence of macroscopic quantum effects in these materials. Quantum tunnelling of the phase leads to fluctuating voltage across the junctions which excites the low energy quasi-particles specific for *d*-wave junctions, causing decoherence. Contributions to dissipation due to different transport processes, such as channels due to nodal quasiparticles, midgap states, or their combination, have been identified and distinguished [32–35]. In particular cases, decoherence times and quality factors were calculated considering the system coupled to an Ohmic heat bath. It has also been argued that problems in observing quantum effects due to the presence of gapless quasi-particle excitations can be overcome by choosing the proper working phase point [33]. In particular, decoherence mechanisms can be reduced by selecting appropriate tunnelling directions because of the strong phase dependence of the quasiparticle conductance in a *d*-wave GB junction.

The search of macroscopic quantum effects become feasible once high quality HTS Josephson junctions [36,37] with significant hysteresis in the current-voltage characteristics were available. We can distinguish two classes of experiments, which are based on two different complementary types of junctions: 1) MQT and ELQ [30,31] on off-axis YBCO grain boundary biepitaxial *JJ*s, where the experiment has been designed to study *d*-wave effects with a lobe of the former electrode facing the node of the latter; 2) MQT and ELQ on intrinsic junctions on single crystals of different materials [38,39], where *d*-wave are expected to play a minor role [33,34]. The experiments using GBs are more complicated because of the complexity of these junctions, but are very complete and allow to address relevant issues on the effects of a *d*-wave OPS on dissipation and coherence. Only GBs junctions can be more easily integrated into circuits.

The GB biepitaxial junctions [40,41] used in [30,31] had reproducible hysteretic behavior up to 90%. A specific feature of these structures is the use of a (110)-oriented CeO_2 buffer layer, deposited on (110) $SrTiO_3$ substrates. YBCO grows along the [001] direction on the CeO_2 seed layer, while it grows along the [103]/[013] direction on $SrTiO_3$ substrates [41,42]. The presence of the CeO_2 pro-

duces an additional 45° in-plane rotation of the YBCO axes with respect to the in-plane directions of the substrate (Fig. 2,*a*). Atomically flat interfaces can be achieved in appropriate conditions [40]. As a consequence, the GBs are the product of two 45° rotations, a first one around the *c*-axis, and a second one around the *b*-axis. This configuration produces a 45° misorientation between the two electrodes to enhance *d*-wave order parameter effects, by varying the interface orientation.

In addition the possibility to tune the critical current I_C through the interface orientation θ in complete agreement with the predictions of a *d*-wave OPS (see Fig. 2,*b*) [41] allows to select the junction for the MQT experiment knowing the OPS configuration exactly. Specific angle orientations can favor both junctions with a Fraunhofer-like pattern (Fig. 2,*c*) and the spontaneous generation of fractional vortices (Fig. 2,*d*) [43,37]. The suitable junction can be therefore selected for the experiment. Since the interest was mostly focused in those features that are distinct from the case of low T_c superconductor (LTS) junctions, namely effects due to OPS, and dissipation due to low energy quasi-particles, the junction in the tilt configuration (angle $\theta = 0°$) turns out to be the most interesting case for the MQT and ELQ experiments. This configuration (lobe to node) maximizes *d*-wave induced effects and allows explore the effects of low energy quasi-particles.

Some new features of Josephson dynamics could be accessible in HTS junction configurations, as, for instance, the role of Andreev bound states [44] and the intrinsic doubly degenerate fundamental state [36,37]. The last is due to unconventional Josephson Current-Phase Relation (CPR) which shows the presence of higher harmonics $(\sin 2\varphi)$ caused by the *d*-wave symmetry of the order parameter [45]. The dynamics of a current biased *JJ* also strongly depends also on the CPR. Up to now, the junction features, which induce the $\sin 2\phi$ component, are not unambiguously identified in a system characterized by a faceting of the grain boundary line [45]. A detailed description of the features of a *JJ* assuming the presence of both first and second harmonic components in the CPR (we neglect higher harmonics due to our low junction barrier transparency) is outside the scope of this review [30,46].

3.1. Experiments on YBCO *biepitaxial Josephson junctions*

We follow [30] and [31] in reporting on the first experimental measurements on MQT in HTS *JJ*s, where all details can be found. The escape rate of the superconducting phase ϕ from a local minimum in the washboard potential into the running state as a function of temperature has been investigated in analogy with experiments on low-T_c junctions. Figure 3 shows a set of switching current probability distributions as a function of temperature for the biepitaxial *JJ*. In the inset of Fig. 3 the switching current probability distribution measured at $T = 0.019$ K is reported along with the original *I–V*.

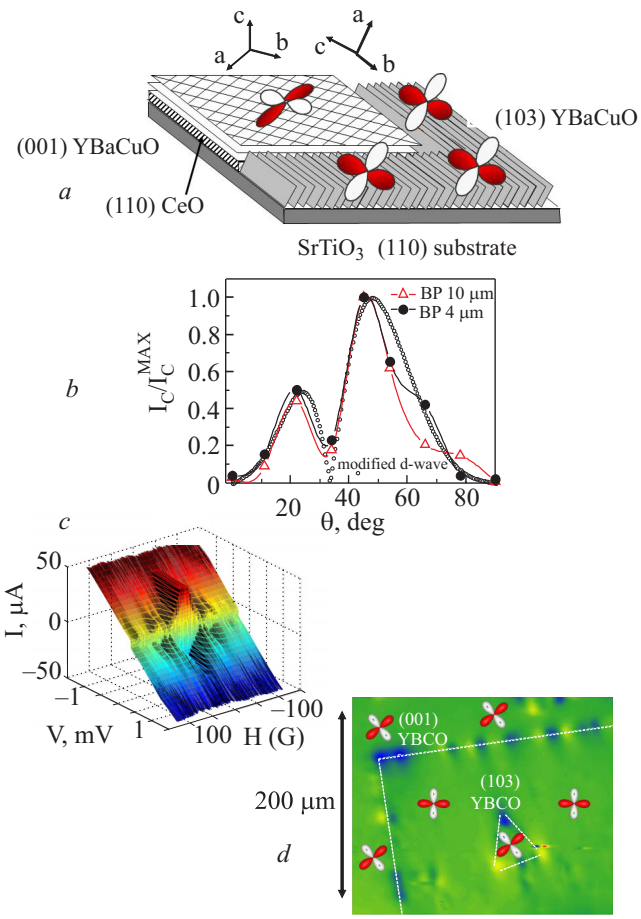

Fig. 2. (*a*) Sketch of the grain boundary structures in biepitaxial CeO_2 (*b*)-based out-of-plane biepitaxial junctions. The presence of the CeO_2 produces an additional 45° in-plane rotation of the YBCO axes with respect to the in-plane directions of the substrate. (*b*) Normalized critical current density J_C vs angle θ for two sets of *c*-axis tilt biepitaxial YBCO junctions, with width 10 μm (triangles) and 4μm (stars). The solid lines connecting the symbols are guides to the eye. The dotted line is the Sigrist–Rice-like formula assuming pure $d_{x^2-y^2}$ pairing symmetry in this geometry [41]. In the bottom inset the scheme of the junction is reported for three different angles, along with the *d*-wave profiles of the two electrodes Adapted from [41]. (*c*) *I–V* curves as a function of the magnetic field. A Fraunhofer profile of the critical current is visible. The misorientation angle is in this case 60°. (*d*) Scanning SQUID microscope image of a 200×200 μm^2 area, enclosing tilt-tilt and twist-tilt in CeO_2-based biepitaxial GBs.The GBs are marked by the presence of spontaneous currents. The sample was cooled and imaged at $T = 4.2$ K in nominally zero field. Adapted from [43].

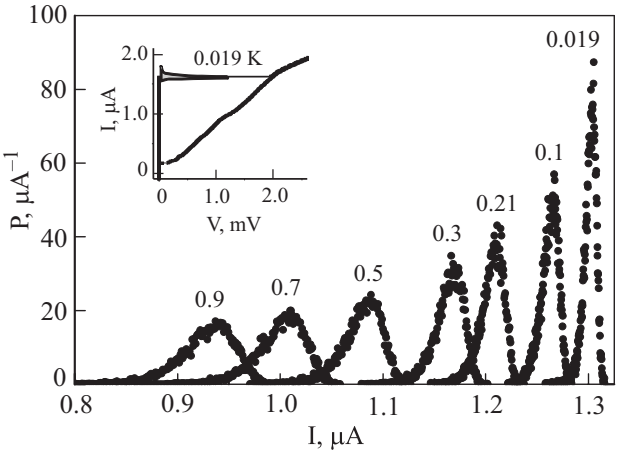

Fig. 3. Switching current probability distribution for $I_{C0} = 1.40$ μA at $B = 0$ T for different bath temperatures T_{bath}. In the inset the switching current probability distribution measured at $T = 0.019$ K is reported along with the original *I–V*. Adapted from Bauch et al. [30].

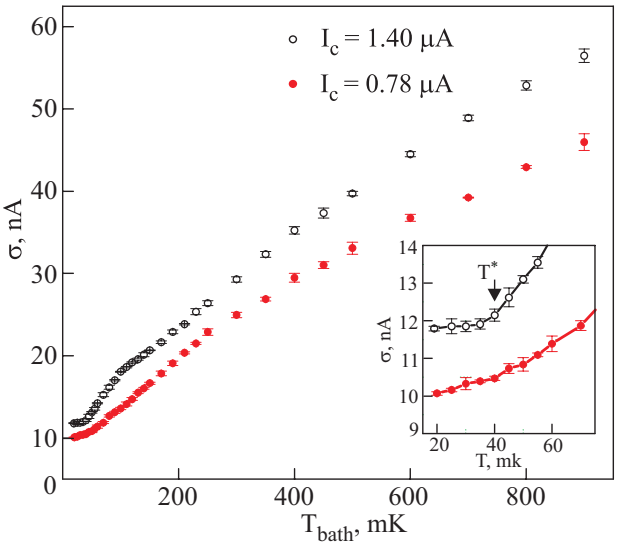

Fig. 4. The measured σ saturates below 50 mK, indicating a crossover from the thermal to the quantum regime. The width σ for $B = 2$ mT and the data for $B = 0$ mT are shown in the inset. Adapted from Bauch et al. [30].

The measured σ saturates below 50 mK, indicating a crossover from the thermal to the MQT regime. An estimation of $R \simeq 100\ \Omega$ results for the electrode impedance using a microstrip transmission line model and $C_S \simeq 1.6$ pF (which is not far from the rough estimate of C obtained from the hysteresis in the dc-*I–V* curve [47]). An estimation of C_J can be obtained by using Eq. (2) in MQT regime [48]. The extracted $C_J \sim 0.22$ pF value gives a plasma frequency $\omega_P / 2\pi \simeq 2.6$ GHz and a quality factor larger than 1 in the quantum regime. The observed crossover temperature ($T \simeq 50$ mK) between the thermal and the quantum regimes is consistent with the predicted values from $T_c^{1D} \simeq (\hbar\omega_P / 2\pi k_B)$ [13,48].

To rule out that the saturation of σ is due to any spurious noise or heating in the measurement setup the switching current probability distributions were measured for a reduced critical current ($I_{C0} = 0.78$ A) by applying an external magnetic field $B = 2$ mT. The width for $B = 2$ mT are shown in the inset of Fig. 4. The data in the presence of a magnetic field clearly show a smaller width, which does not saturate down to the base temperature.

In the temperature regime between 50 and 100 mK the data start to follow the well known $\sigma^{2/3}$ dependence due to thermal escape [49] (see the dashed line in Fig. 4). However, for $T \sim 110$ mK there is an hump, i.e., a transition to a $\sigma^{2/3}$ dependence with lower values of (solid line). These larger values in the low temperature region correspond to an enhanced thermal escape rate. A possible explanation of this effect is the onset of a second harmonic component in the CPR at low temperatures, due to the low junction barrier transparency [30].

Apart from being one of the keys to have low barrier transparency, another important consequence of *c*-axis tilt is the presence of a significant kinetic inductance in the modeling of YBCO *JJ*. Indeed, in these junctions the presence of a kinetic inductance and a stray capacitance determine the main difference in the washboard potential making the system behavior depending on two degrees of freedom [31]. The YBCO *JJ* is coupled to this *LC*-circuit (Fig. 5,*a*) and the potential become two-dimensional (2D). Similar behavior has been observed in a low-T_C *dc* superconducting quantum interference device [50].

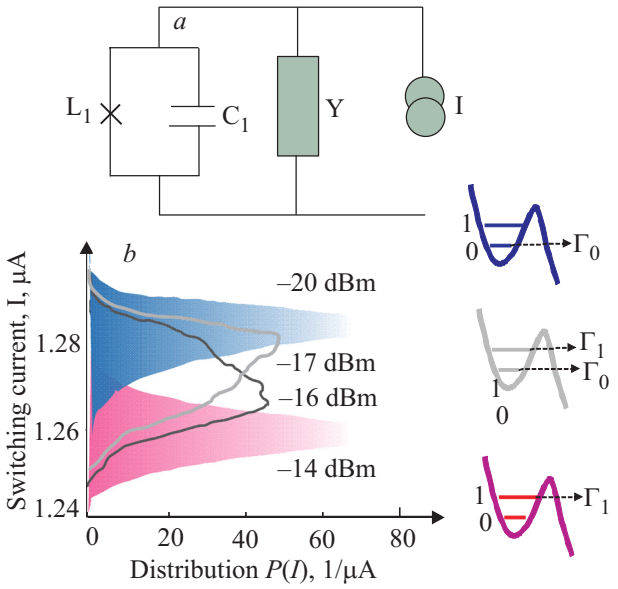

Fig. 5: Measured switching current probability distribution $P(I)$ in presence of microwaves at a frequency of 850 MHz and temperature $T = 15$ mK. The applied power at the room temperature termination varies from –20 to –14 dBm. On the right the MQT processes correspond to the switching current probability distribution $P(I)$. Adapted from Bauch et al. [31]

The coupling with LC can be described by the following 2D potential [48,51]:

$$U(\phi,\phi_S)/E_J = \frac{1}{2\beta}(\phi_j-\phi_S)^2 - \gamma\phi_S - \cos\phi_j$$

where $\phi_S = \phi_j + (2\pi/\Phi_0)I_S L_S$ is the phase difference across the shunt capacitor C_S and I_S the current in the inductance L_S. It has been shown that the barrier height ΔU is the same found in the 1D case [51,48]. The 2D potential modifies the value of the crossover temperature and, in general, of both thermal and MQT escape rates. In particular in the experiment reported in [31] the *LC* values was $L_S \simeq 7.2(\Phi_0/2\pi I_{C0} = 7.2 L_J 0)$ and $C_S \simeq 7.3 C_J$.

In analogy to the LTS case the normalized bias current γ is ramped from zero to a value near to 1, at finite temperature, the junction may switch into a finite voltage state for a bias current < 1. This corresponds to the particle escaping from the well either by a thermally activated process or by tunneling through the barrier potential (MQT). In the pure thermal regime, the escape rate for weak to moderate damping $(Q>1)$ is determined by

$$\Gamma_t = a_t^{2D}\frac{\omega_R}{2\pi}\exp\left(-\frac{\Delta U}{k_B T}\right)$$

where $\Delta U = (4\sqrt{2}/3)E_J(1-\gamma)^{3/2}$ is the barrier height for γ close to 1, and ω_R is the attempt frequency in the well. Explicit expression for 2D thermal prefactor a_t^{2D} can be found in [48]. In the limit of large L_S and C_S (as in experiment [31]) this correction is small and it is mainly due to the shift of the attempt frequency which is lower than standard JJ plasma frequency ω_P.

The escape rate will be dominated by MQT at low enough temperature for $Q>1$ the expression for a 2D potential is:

$$\Gamma_q = a_q^{2D}\frac{\omega_P}{2\pi}\exp\left[-\frac{36\Delta U}{5\hbar\omega_P}\left(1+\frac{5L_J}{2L_S}\right)\right]$$

where $a_q = \left[864\pi(\Delta U/\hbar\omega_P)\left(1+\frac{5L_J}{2L_S}\right)\right]^{1/2}$. So the MQT rate is reduced by the factor $5L_J/2L_S$ [48]. From above Eqs. (1) and (2) also an expression for $\sigma(T)$ the HMFW of $P(I)$ switch distribution can be numerically calculated and compared with experiments.

The theory reported in Ref. 48 is in excellent agreement with experimental escape rates, though, at the moment, cannot explain the hump structure of σ near 0.1 K. The problem can be related to a correct description of dynamical/thermal population of excited states in the metastable well, at present neglected in the *LC*-circuit model [48].

The *LC*-circuit model, the so-called «shell» circuit, is also of great importance to explain the Energy Level Quantization (ELQ) experiment reported in Ref. 31. Microwaves at frequency ω_{rf} were transmitted to the junction via a simple dipole antenna at a temperature below T_c. When ω_{rf} of the incident radiation (or multiples of it) coincides with the bias current-dependent level separation of the junction, $\nu_{10}(\gamma) = m\omega_{rf}$, the first excited state is populated. Here, m is an integer number corresponding to an *m*-photon transition from the ground state to the first excited state. Fig. 5,*b* shows the evolution of the switching-current histogram as a function of the applied microwave power for the $m=3$ three photon process.

At low power values (–20 dBm), the escape is basically from the ground state, since the occupation probability of the first excited state is negligible. When the applied power is increased (–17 dBm and –16 dBm), the first excited state starts to be populated. Then in the histogram two peaks appear corresponding to tunneling from both the first excited Γ_1 and ground Γ_0 states. The escape from the first excited state is exponentially faster and dominates, and the switching current distribution is again single peaked at –14 dBm. From the Lorentzian-shape of the escape rate, a Q value of the order of 40 is extracted [31], comparable with the first best results obtained in LTS junctions.

Specific effects related to stray capacitance and large kinetic inductance have been discussed both in the original paper [31] and in subsequent papers [48].

The observation of quantum tunneling, narrow width of excited states, and a large Q value support the notion of «quiet» qubits based on *d*-wave symmetry superconductor, but the meaning of the experiments goes beyond. There may be some mechanism preventing the low-lying quasiparticles in the *d*-wave state from causing excessive dissipation. It could be also supposed the presence of some kind of condensation mechanism of quasiparticles, in general agreement with the HTS SU(2) slave-boson model, where the physical properties of the low lying quasiparticles are found to resemble those in BCS theory [52]. The existence of a subdominant imaginary *s*-wave component of the order parameter inducing a gapped excitation spectrum could be another possible explanation, probably more related to the presence of the junction interface. This last possibility has been discussed in various experiments available in literature, but there is neither a convincing reproducible proof nor a neat definition of the controllable experimental conditions which lead to this effect [36,37].

4. Mesoscopic effects and coherence in HTS nanostructures

Nanotechnology can provide another path to study coherence and quasi-particle relaxation processes in HTS. The ultimate limit of GB performances also in terms of yield and reproducibility, will be possibly achieved when

junction dimensions get closer to the characteristic scaling lengths of HTS (i.e., coherence length, charge domains, and so on) and to the typical size of GB facets, which are one of the main sources of the lack of uniformity of the transport properties of GBS junctions. Nanoscale junctions have therefore full potentials to isolate intrinsic features of HTS systems, and represent the ideal tool to better address the interesting topic of coherence in strongly correlated *d*-wave superconductors. Benefits will be obviously extended to applications based on HTS junctions.

The first studies on bicrystal submicron *JJ*s have given encouraging results as the reduction of decoherence [53], the presence of the 2φ component [54], and of Andreev bound states [55].

Recently submicron biepitaxial junctions have been realized down to about 500 nm by using both *e*-beam lithography and C and Ti masking [56]. This step is even more significant because applied to the off-axis biepitaxial junctions, which have shown the macroscopic quantum effects, and to be sensitive to directional transport along the lobes or the nodes of the *d*-wave OPS. Yield and reproducibility have been improved on this width scale. These improvements reflect the advances registered in patterning simple nanobridges, which have been reproducibly scaled on *c*-axis YBCO down to about 100 nm [57]. Studies on flux dynamics have been also realized in nanorings of inner and external radius of about 150 nm and 300 nm, respectively [58].

This classical controllable «top-down» approach is going to be accompanied by some sort of «bottom-up» techniques, which fund on the intrinsic nature of GB. The complex growth process may determine self-assembled nanochannels of variable dimensions, ranging typically from 20 nm to 200 nm, often «enclosed» in macroscopic impurities. Even if this very last technique is not ideal on the long range for applications, since it needs an additional critical step to locate the nanobridges and etch the HTS thin film, it can be really helpful to understand the ultimate limit of the junction performances and to understand the transport mechanisms.

An example of how to use the natural self-assembling to extract information on the physics of HTS Josephson junctions, has been recently given on a study on universal conductance fluctuations (UCF) in magnetic field in YBCO biepitaxial Josephson junctions. This is of relevance to investigate coherent quantum behavior in HTS [59,60]. Structural investigations allow first to locate macroscopic impurities which enclose the conducting channel, whose size is roughly confirmed by the period of the magnetic pattern of the critical current. At low temperatures, quantum coherence can be monitored in the conductance G of a normal metallic sample of length L_x attached to two reservoirs [61,62]. The electron wave packets that carry current in a diffusive wire have minimum size of the order of $L_T > L_x >> l$. Here l is the electron mean free path in the wire and L_T is the thermal diffusion length (D is the diffusion constant). The first inequality is satisfied at relatively low temperatures as far as $k_B T << \varepsilon_C \approx \hbar D / L_x^2$ being ε_C the Thouless energy. Conductance fluctuations become appreciable at low temperatures, in the whole magnetic field range. At low voltages ($eV << \varepsilon_C$), the system is in the regime of universal conductance fluctuations: the variance $< g^2 >$ of the dimensionless conductance $g = G/(2e^2/\hbar)$ is of order of unity. The fluctuations are nonperiodic, and have all the typical characteristics of mesoscopic fluctuations [61,62]. Studies have been carried out at different voltages and non-equilibrium conditions. An energy scale of the order of 1 meV arises naturally from the analysis of the autocorrelation function of the conductance as a function of the voltage [59,60]. This has been identified as the Thouless energy ε_C, and its value is consistent with a size of the channel of the order of 100 nm. This is proportional to the inverse time an electron spends in moving coherently across the mesoscopic sample. Quasi-particles seem to travel coherently across the junction even if $V >> \varepsilon_C$. Hence, microscopic features of the weak link appear as less relevant, in favor of mesoscopic, non local properties. In this case, the quasi-particle phase coherence time τ_φ does not seem to be limited by energy relaxation due to voltage induced nonequilibrium. The remarkably long lifetime of the carriers, found in these experiments, appears to be a generic property in high-T_C YBCO junctions as proved by optical measurements [63] and by macroscopic quantum tunneling [30,31].

5. Conclusions

The great interest of the results reviewed in this chapter lies in the combination of the stimulating subject of macroscopic quantum phenomena (MQT, ELQ) with the new important clues that such phenomena provide on underlying aspects of the physics of HTS. We have focused on macroscopic quantum decay phenomena, as one of the most exciting expressions of the Josephson effect. A system which displays macroscopic quantum effects despite the presence of nodes in the order parameter symmetry and therefore of low energy quasi-particles, raises several challenging issues on dissipation mechanisms and on the peculiar coherence phenomena occurring in Josephson systems and in HTS. We believe that the progress in quantum engineering and in nanotechnologies will represent an invaluable additional drive force to further address advanced topics on the Josephsin effect and on macroscopic quantum phenomena. Once the true «intrinsic» transport channels across junctions are controlled and isolated from «extrinsic» contributions, which result from the complex morphology of the junctions (faceting, and so on), not only we will get closer to the basic features of HTS (possibly stripes, spin-charge separation, ...) but we will be also entitled to have a more complete scenario on the Josephson effect, analogies and differences between HTS and LTS *JJ*s [1–5].

We acknowledge support from EC Strep Project MIDAS–Macroscopic Interference Devices for Atomic and Solid State Physics: Quantum Control of Supercurrents.

We would like to thank Thilo Bauch, John R. Kirtley, Daniela Stornaiuolo and Arturo Tagliacozzo for valuable discussions.

1. B.D. Josephson, *Phys. Lett*. **1**, 251 (1962).
2. P.W. Anderson, *Special Effects in Superconductivity,* in: *Lectures on the Manybody Problem*, E.R. Caianiello (ed.), Vol. **II** p. 113, Academic Press, Ravello (1963).
3. I.O. Kulik and K. Yanson, *The Josephson Effect in Superconductive Tunneling Structures* (Israel Program of Scientific Translations), Jerusalem (1972).
4. A. Barone and G. Paternó, *Physics and Applications of the Josephson Effect*, John Wiley, New York (1982).
5. K.K. Likharev, *Dynamics of Josephson Junctions and Circuits,* Gordon and Breach, New York (1986); K.K. Likharev, *Rev. Mod. Phys*. **51**, 101 (1979).
6. A. Barone, *Weakly Coupled Macroscopic Quantum Systems: Likeness with Difference*, I.O. Kulik and R. Ellialtioglu (eds.), Kluwer Academic Publishers (2000), p. 301.
7. D.J. Van Harlingen, *Rev. Mod. Phys*. **67**, 515 (1995).
8. C.C. Tsuei and J.R. Kirtley, *Rev. Mod. Phys*. **72**, 969 (2000) and Refs. reported therein.
9. S. Coleman, *Phys. Rev*. **D15**, 2929 (1977).
10. A.J. Leggett, *Macroscopic Quantum Systems and the Quantum Theory of Measurements*, *Supplement of Prog. Theor. Phys*. **69**, 80 (1980); A.J. Leggett, *Quantum Tunneling of a Macroscopic Variable in Quantum Tunneling in Condensed Media*, Yu. Kagan and A.J. Leggett (eds.), Elsevier Science Publ. (1992) and Refs. reported therein.
11. Yu.M. Ivanchenko and L.A. Zilberman, *Sov. Phys. JETP* **28**, 1272 (1969).
12. A.O. Caldeira and A.J. Leggett, *Phys. Rev. Lett*. **46**, 211 (1981).
13. H. Grabert and U. Weiss, *Phys. Rev. Lett*. **53**, 1787 (1984).
14. A.I. Larkin and Yu.N. Ovchinnikov, *Zh. Eksp. Teor. Fiz*. **85**, 1510 (1983) [*Sov. Phys. JETP* **58**, 876 (1983)]; *Phys. Rev*. **B28**, 828 (1983).
15. A. Barone and Yu.N. Ovchinnikov, *J. Low Temp. Phys*. **55**, 297 (1984); Yu.N. Ovchinnikov and A. Barone, *J. Low Temp. Phys*. **67**, 323 (1987); A. Barone, *J. Supercond*: *Incorporating Novel Magnetism* **17**, 585 (2004).
16. R.F. Voss and R.A. Webb, *Phys. Rev. Lett*. **47**, 265 (1981); L.D. Jackel, J.P. Gordon, E.L. Hu, R.E. Howard, L.A. Fetter, D.M. Tennant, R.W. Epworth, and J. Kurkijarvi, *Phys. Rev. Lett*. **47**, 697 (1981); S. Washburn, R.A. Webb, R.F. Voss, and S.M. Farris, *Phys. Rev. Lett*. **54**, 2712 (1985); D.B. Shwartz, B. Sen, C.N. Archie, and J.E. Lukens, *Phys. Rev. Lett*. **54**, 1547 (1985); M.H. Devoret, J.M. Martinis, and J. Clarke, *Phys. Rev. Lett*. **55**, 1908 (1985); W. der Boer and R. de Bruyn Ouboter, *Physica* **98B**, 185 (1980); D.W. Bol, R. van Weelderen and R. de Bruyn Ouboter, *Physica* **122B**, 2 (1983); D.W. Bol, J.J.F. Scheffer, W. Giele, and R. de Bruyn Ouboter, *Physica* **113B**, 196 (1985); R.J. Prance, A.P. Long, T.D. Clarke, A. Widom, J.E. Mutton, J. Sacco, M.W. Potts, G. Negaloudis, and F. Goodall, *Nature* **289**, 543 (1981); I.M. Dimitrenko, V.A. Khlus, G.M.Tsoi, and V.I. Shnyrkov, *Fiz. Nizk. Temp*. **11**, 146 (1985) [*Sov.J. Low Temp. Phys*. **11**, 77 (1985)]; J.M. Martinis, M.H. Devoret, and J. Clarke, *Phys. Rev*. **B35**, 4682 (1987); U. Weiss, H. Grabert, and S. Linkwitz, *J. Low Temp. Phys*. **68**, 213 (1987).
17. *Josepshon Effect-Achievements and Trends* ISI-85 *Torino*, A. Barone (ed.) World Scientific (1985) and Refs. reported therein.
18. A.J. Leggett, S. Chakravarty, A.T. Dorsey, M.P.A. Fischer, A. Garg, and W. Zwerger, *Rev. Mod. Phys*. **59**, 1 (1987).
19. J. Clarke, A.N. Cleland, M.H. Devoret, D. Esteve, and J.M. Martinis, *Science* **29**, 992 (1988).
20. A.V. Zhuravlev and A.B. Zorin, *Fiz. Nizk. Temp*. **16**, 184 (1990) [*Sov. J. Low Temp. Phys*. **16**, 102 (1990)]; J.M. Schmidt, A.N. Cleland, and J. Clarke, *Phys. Rev*. **B43**, 229 (1991).
21. R. Rouse, S. Han, and J.E. Lukens, *Phys. Rev*. **B75**, 1614 (1995).
22. C. Cosmelli, P. Carelli, M.G. Castellano, F. Chiariello, G.D. Palazzi, R. Leoni, and G. Torrioli, *Phys. Rev. Lett*. **82,** 5357 (1999). For aspects of the sample preparation see also M.G. Castellano et al. *J. Appl. Phys*. **80**, 2928 (1996).
23. Y. Nakamura, Y. Pashkin, and J.S. Tsai, *Nature* **398**, 786 (1999).
24. J.R. Friedman, V. Patel, W. Chen, S.K. Tolpygo, and J.E. Lukens, *Nature* **406**, 43 (2000).
25. L.B. Ioffe, V.B. Geshkenbein, M.V. Feigel'man, A.L. Fauchere, and G. Blatter, *Nature* **398**, 679 (1999); C.C. Tsuei and J.R. Kirtley, *Physica* (Amsterdam) **367C**, 1 (2002); B. Doucot, M.V. Feigel'man, and L.B. Ioffe, *Phys. Rev. Lett*. **90**, 107003 (2003).
26. A.Yu. Kitaev, *preprint quant-ph/9707021 at xxx.lanl.gov*, (1997).
27. G. Blatter, V.B. Geshkenbein, and L.B. Ioffe, *Phys. Rev*. **B63**, 174511 (2001).
28. A. Wallraff, A. Lukashenko, J. Lisenfeld, A. Kemp, M.V. Fistul, Y. Koval, and A.V. Ustinov, *Nature*, **425**, 155, (2003).
29. A. Kemp, A. Wallraff, and A.V. Ustinov, *Phys. Status Solidi* **233**, 472 (2002).
30. T. Bauch, F. Lombardi, F. Tafuri, G. Rotoli, A. Barone, P. Delsing, and T. Cleason, *Phys. Rev. Lett.* **94**, 087003 (2005).
31. T. Bauch, T. Lindström, F. Tafuri, G. Rotoli, P. Delsing, T. Claeson, and F. Lombardi, *Science* **311**, 5757 (2006).
32. Y.V. Fominov, A.A. Golubov, and M.Y. Kupriyanov, *JETP Lett*. **77**, 587 (2003).
33. M.H.S. Amin and A.Y. Smirnov, *Phys. Rev. Lett*. **92**, 017001 (2004).
34. S. Kawabata, S. Kashiwaya, Y. Asano, and Y. Tanaka, *Phys. Rev*. **B70**, 132505 (2004).
35. S. Kawabata, S. Kashiwaya, Y. Asano, and Y. Tanaka, *Phys. Rev*. **B72**, 052506 (2005); T. Yokoyama, S. Kawabata, T. Kato, and Y. Tanaka, *Phys. Rev*. **B76**, 134501 (2007).
36. H. Hilgenkamp and J. Mannhart, *Rev. Mod. Phys*. **74**, 485 (2002).

37. F. Tafuri and J.R. Kirtley, *Rep. Prog. Phys*. **68**, 2573 (2005).
38. K. Inomata, S. Sato, K. Nakajima, A. Tanaka, Y. Takano, H. B. Wang, M. Nagao, H. Hatano, and S. Kawabata, *Phys. Rev. Lett.* **95**, 107005 (2005).
39. X.Y. Jin, J. Lisenfeld, Y. Koval, A. Lukashenko, A.V. Ustinov, and P. Mueller, *Phys. Rev. Lett*. **96**, 177003 (2006).
40. F. Tafuri, F. Miletto Granozio, F. Carillo, A. Di Chiara, K. Verbist, and G. Van Tendeloo, *Phys. Rev*. **B59**, 11523 (1999).
41. F. Lombardi, F. Tafuri, F. Ricci, F. Miletto Granozio, A. Barone, G. Testa, E. Sarnelli, J.R. Kirtley, and C.C. Tsuei, *Phys. Rev. Lett*. **89**, 207001 (2002).
42. F. Miletto Granozio, U. Scotti di Uccio, F. Lombardi, F. Ricci, F. Bevilacqua, G. Ausanio, F. Carillo, and F. Tafuri, *Phys. Rev*. **B67**, 184506 (2003).
43. F. Tafuri, J.R. Kirtley, F. Lombardi, and F. Miletto Granozio, *Phys. Rev*. **B67**, 174516 (2003).
44. C.-R. Hu, *Phys. Rev. Lett*. **72**, 1526 (1994); T. Löfwander, V.S. Shumeiko, and G. Wendin, *Supercond. Sci. Technol*. **14**, R53 (2001); S. Kashiwaya and Y. Tanaka, *Rep. Prog. Phys*. **63**, 1641 (2000).
45. E. Ilichev, V. Zakosarenko, R.P.J. Ijsselsteijn, H.E. Hoenig, V. Schultze, H.G. Meyer, M. Grajcar, and R. Hlubina, *Phys. Rev*. **B60**, 3096 (1999); E.E. Il'ichev, M. Grajcar, R. Hlubina, R.P.J. IJsselsteijn, H.E. Hoenig, H.-G. Meyer, A. Golubov, M.H.S. Amin, A.M. Zagoskin, A.N. Omelyanchouk, and M.Yu. Kupriyanov, *Phys. Rev. Lett*. **86**, 5369 (2001); T. Lindstrom, S.A. Charlebois, A.Ya. Tzalenchuk, Z. Ivanov, M.H.S. Amin, and A.M. Zagoskin, *Phys. Rev. Lett*. **90** 117002 (2003).
46. The dynamics of a *JJ* can be described by assuming the presence of both first and second harmonic components in the CPR (higher harmonics can be neglected because of low junction barrier transparency). defining $I = I_1(\sin\phi - a\sin 2\phi)$ where $a = I_2 / I_1$, and I_2 and I_1 are the second and first harmonic components. At a given value of *a*, the dynamics is equivalent [47] to that of a particle of mass m_ϕ moving in a washboard potential $U(a) = -(I_1\Phi_0 / 2\pi)((I_{C0} / I_1)\gamma\phi + \cos - (a/2)\cos 2\phi)$, where $E_1 = I_1\Phi_0 / 2\pi$ is the first harmonic of the Josephson energy and Φ_0 is the flux quantum. The normalized bias current $\gamma = I / I_C 0$ determines the tilt of the potential, where $I_{C0} = I_1 \max(\sin\phi - a\sin 2\phi)$ is the maximum critical current of the *JJ*. For zero bias and $a > 0.5$ the potential has the shape of a double well. In the case $0.5 < a < 2$ the phase will always escape into the running state from the lower lying well of the tilted double-welled washboard potential, as could be confirmed by performing numerical simulations of the Langevin equation of motion. More details can be found in: A.Ya. Tzalenchuk, T. Lindström, S.A. Charlebois, E.A. Stepantsov, Z. Ivanov, and A.M. Zagoskin, *Phys. Rev*. **B68**, 100501 (2003).
47. W.C. Stewart, *Appl. Phys. Lett*. **12**, 277 (1968); D.E. McCumber, *J. Appl. Phys*. **39,** 3113 (1968).
48. S. Kawabata, T. Bauch, and T. Kato, *Phys. Rev*. **B80**, 174513 (2009).
49. L.D. Jackel, J.P. Gordon, E.L. Hu, R.E. Howard, L.A. Fetter, D.M. Tennant, R.W. Epworth, and J. Kurkijärvi, *Phys. Rev. Lett*. **47**, 697 (1981).
50. F. Balestro, J. Claudon, J.P. Pekola, and O. Buisson, *Phys. Rev. Lett*. **91**, 158301 (2003).
51. G. Rotoli, T. Bauch, T. Lindström, D. Stornaiuolo, F. Tafuri, and F. Lombardi, *Phys. Rev*. **B75**, 144501 (2007).
52. X.G. Wen and P.A. Lee, *Phys. Rev. Lett*. **80**, 2193 (1998).
53. A.Ya. Tzalenchuk, T. Lindström, S.A. Charlebois, E.A. Stepantsov, Z. Ivanov, and A.M. Zagoskin, *Phys. Rev*. **B68**, 100501 (2003).
54. E. Il'ichev, M. Grajcar, R. Hlubina, R.P.J. IJsselsteijn, H.E. Hoenig, H.-G. Meyer, A. Golubov, M.H.S. Amin, A.M. Zagoskin, A.N. Omelyanchouk, and M.Yu. Kupriyanov, *Phys. Rev. Lett*. **86**, 5369 (2001).
55. G. Testa, A. Monaco, E. Esposito, E. Sarnelli, D.J. Kang, S.H. Mennema, E.J. Tarte, and M.G. Blamire, *Appl. Phys. Lett.* **85**, 1202 (2004); G. Testa, E. Sarnelli, A. Monaco, E. Esposito, M. Ejrnaes, D.J. Kang, S.H. Mennema, E.J. Tarte, and M.G. Blamire, *Phys. Rev*. **B71**, 134520 (2005).
56. D. Stornaiuolo, G. Rotoli, K. Cedergen, T. Bauch, F. Lombardi, and F. Tafuri, *to be published* in *J. Appl. Phys*. (2010); D. Stornaiuolo, E. Gambale, T. Bauch, D. Born, K. Cedergren, D. Dalena, A. Barone, A. Tagliacozzo, F. Lombardi, and F. Tafuri, *Physica* **C468**, 310 (2008).
57. G. Papari, F. Carillo, D. Born L. Bartoloni, E. Gambale, D. Stornaiuolo, P. Pingue, F. Beltram, and F. Tafuri, *IEEE Trans. on Appl. Supercond*.**19**, 183 (2009).
58. F. Carillo, G. Papari, D. Stornaiuolo, D. Born, D. Montemurro, P. Pingue, F. Beltram, and F. Tafuri, *Phys. Rev*. **B81**, 054505 (2010).
59. A. Tagliacozzo, D. Born, D. Stornaiuolo, E. Gambale, D. Dalena, F. Lombardi, A. Barone, B.L. Altshuler, and F. Tafuri, *Phys. Rev*. **B75**, 012507 (2007).
60. A. Tagliacozzo, F. Tafuri, E. Gambale, B. Jouault, D. Born, P. Lucignano, D. Stornaiuolo, F. Lombardi, A. Barone, and B.L. Altshuler, *Phys. Rev*. **B79**, 024501 (2009).
61. B.L. Altshuler and A.G. Aronov, in: *Electron-Electron Interaction in Disordered Systems*, A.L. Efros and M. Pollak Elsevier (eds.), Amsterdam (1985); P.A. Lee and T.V. Ramakrishnan, *Rev. Mod. Phys*. **57**, 287 (1985); P.A. Lee and A.D. Stone, *Phys. Rev. Lett*. **55**, 1622 (1985); P.A. Lee, A.D. Stone, and H. Fukuyama, *Phys. Rev*. **B35**, 1039 (1987); B. Al'tshuler and P. Lee, *Phys. Today* **41**, 36 (1988); R.A. Webb and S. Washburn, *Phys. Today* **41**, 46 (1988); For a review see *Mesoscopic Phenomena in Solids*, B.L. Altshuler, P.A. Lee, and R.A. Webb (eds.), North-Holland, New York, (1991).
62. Y. Imry, *Introduction to Mesoscopic Physics,* Oxford University Press (1997).
63. N. Gedik, J. Orenstein, R. Liang, D.A. Bonn, and W.N. Hardy, *Science* **300**, 1410 (2003).